Modelling Fringe Projection Based on Linear Systems Theory and Geometric Transformation

George Gayton*, Rong Su and Richard Leach
University of Nottingham, Manufacturing Metrology Team, Advanced Manufacturing Building, Jubilee Campus, Nottingham, NG8 1BB, UK
** Corresponding author: george.gayton@nottingham.co.uk*

Keywords: fringe projection, diffraction, surface topography, metrology, uncertainty

Abstract. Fringe projection measurement techniques offer fast, non-contact measurements of the surface form of manufactured parts at relatively low cost. Recent advances in fringe projection have reduced measurement errors from effects such as multiple surface reflections and projector defocus. However, there is no standardised calibration framework for fringe projection systems and an uncertainty estimation of surface measurements is rarely carried out in practice. A calibration framework for estimating spatial frequency-dependent measurement uncertainty built on solid theoretical foundations is required. To move towards traceable surface measurement using fringe projection techniques, we are developing a measurement model to accurately predict the captured image and include all major uncertainty contributors, i.e. a virtual fringe projection system. The first step of the model is to calculate the optical field distribution using the three-dimensional optical transfer function of the projector. Next, a camera image is built up using a ray-tracing model to probe the optical field distribution at the measurement surface boundary. The results are compared to an experimental fringe projection system. The intention is to use this model within a Monte-Carlo framework to move towards estimating the uncertainty at each point-cloud data point.

Introduction

Fringe projection is a three-dimensional optical measurement technique that measures surface topography and geometrical dimensions of a part and has seen increased use in the aerospace, automotive and medical industries [1, 2]. Fringe projection offers relatively fast measurements in the form of high-density point clouds using relatively cost-effective components: a camera and a projector. A pattern is projected onto a measurement surface. The camera, offset from the projector records the image of the projected pattern, which has become distorted due to the surface geometry. The image is decoded to give correspondence between the reference frame of the camera and the projector, allowing points to be triangulated between the images. Many different fringe projection techniques exist which project different patterns, all optimised for specific measurement scenarios [3, 4].

Unlike conventional contact measurement methods, e.g. coordinate measuring machines (CMMs), there is no standardised calibration framework for fringe projection systems. Uncertainty evaluation of fringe projection surface measurements is rarely carried out in practice, restricting the use of this technique in manufacturing industry. The dependence of fringe projection measurements on surface characteristics, e.g. optical properties and topography, makes current calibration methods given in ISO 15530 part 1-3 [5] (for contact CMMs) unsuitable for fringe projection. Also, it is unclear how to apply the calibration approach in ISO 25178 [6] for areal surface topography measuring instruments.

Current work on fringe projection systems focuses on limiting the magnitude of certain artefacts, such as global illumination, multiple surface reflections [7-9]. However, few authors quantify the influence of these artefacts on the measurement outcome. This quantification process is difficult in fringe projection systems; any process that alters the intensity of light scattered/reflected from the measurement surface and recorded by the camera will alter the measurement outcome. A rigorous mathematical model is missing that includes the large number of influence factors that can alter the measurement outcome. The model must also work over a large range of measurement scales, since fringe projection systems operate from millimetre-range surface topography measurements [10, 11] to larger scales of metres and above [12].

Previous attempts to simulate fringe projection have been limited to geometrical optics only, ignoring diffraction and surface effects. Surface optical characteristics strongly influence the

measurement outcome [13-15], yet there is no quantitative method for determining the influence of an object's optical characteristics on the final image. Ray tracing is a popular method to simulate complicated scenes but is typically time consuming and does not naturally contain diffraction effects [16]. Recently, there has been some progress in using linear systems theory to understand and model optical surface topography instruments [17-19]. These instruments tend to work at smaller scales, where the numerical aperture (NA) is large enough that diffraction effects are significant within the working measurement volume. Previously, a 2D instrument transfer function was used to characterise the spatial resolution of a fringe projection system [15]. The instrument transfer function was valid with the assumption that the change in surface height was much smaller than the working distance of the camera, and the amplitude of the surface spatial frequency components were smaller than the linearity surface height limits. In this paper, under the assumption of projector shift-invariance and Lambertian scattering, we combine a geometrical and linear systems model to model a fringe projection system.

Method

3D linear filter. The projector in a fringe projection system forms an image of, e.g. a 2D grating pattern, onto the surface of an object. Not all objects of interest fit entirely within the depth of focus of a projection system. Therefore, it is important to know the intensity distribution of the projected pattern in the 3D volume. In this work, we attempt to use 3D imaging theory to model the imaging process in a fringe projection system. Under linear systems theory, the intensity distribution at position $\boldsymbol{r}$ in the projection volume $I_{out}(\boldsymbol{r})$ can be described as

$$I_{out}(\boldsymbol{r}) = I_{in}(\boldsymbol{r}) \otimes h(\boldsymbol{r}), \tag{1}$$

where $I_{in}(\boldsymbol{r})$ and $h(\boldsymbol{r})$ are the input intensity distribution and point spread function respectively. The Fourier transform of Eq. (1) gives

$$\tilde{I}_{out}(\boldsymbol{k}) = \tilde{I}_{in}(\boldsymbol{k}) \times H(\boldsymbol{k}), \tag{2}$$

where $\boldsymbol{k}$ is the spatial frequency vector. Assuming the projector is a shift-invariant and incoherent system, its optical transfer function (OTF), given by $H(\boldsymbol{k})$, is similar to that of a microscope [20].

If the volumetric intensity distribution of the fringe pattern can be predicted using Eq. (1) and the location of the surface is given, light reflected from the surface can be calculated. To simplify the surface scattering problem, a Lambertian surface that scatters uniformly in all angles is assumed. By further assuming the surface is located within the depth of focus of the camera, the image of the fringe pattern recorded by the camera can be calculated by considering the camera modulation transfer function (MTF) and the perspective of the camera.

Geometrical transform. A geometrical transformation (Ξ), is applied to the output field distribution that first expands the output distribution uniformly, then compresses or stretches the distribution in the lateral position (x, y) as a function of the axial position z. The geometrical transformation Ξ is chosen so that $I_{out}(\boldsymbol{r})$ resembles that of a projection system. The expansion is given by

$$\boldsymbol{r}_M = \Xi \boldsymbol{r}, \tag{3}$$

with Ξ given by

$$\Xi = \begin{pmatrix} M^2 z & 0 & 0 \\ 0 & M^2 z & 0 \\ 0 & 0 & M \end{pmatrix} \tag{4}$$

where M is the global magnification of I_{in}. For the total intensity of $I_{out}(\boldsymbol{r})$ across successive planes perpendicular to the optical axis to remain constant, $I_{out}(\boldsymbol{r})$ decreases proportional to the increase in successive plane area.

With the assumption that the scene remains fully within the depth of focus of the camera and that scattering is Lambertian the surface intensity values can be mapped directly to camera pixels to create $I_{cam}(u, w)$. A simple ray tracing algorithm maps surface intensity values to the corresponding pixel. The same algorithm is used to establish occlusions in the projector field of view.

Experimental. A number of images were taken using a simple fringe projection system. Fringes were generated on a Raspberry Pi, projected using an Optoma HD142X projector and captured using a Nikon D3500 camera in a thermally stable environment (within 1ºC change). The laboratory wall was used as a flat plane target as it is a relatively flat, white, Lambertian surface that filled the projector field of view. A set of 20 mm diameter optical spheres were also used as a target. The optical spheres are Al_2O_3 balls with a matte finish, designed to be Lambertian. All images have been manually cropped to remove scenery and converted to grayscale.

Simulation. Two scenes were simulated that created the same features that are found in the experimental images. For the projector, NA = 0.2 and the projector image contains 800×450 pixels. The intensity distribution $I(\boldsymbol{r})$ sampling resolution is 800×450×512. The sample distance for $I_{in}(\boldsymbol{r})$ is set to 2 nm in (x, y). The model is run in MATLAB 2018b, on a computer with 32 GB of memory, Intel Xeon W-2123 with a clock speed 3.6 GHz. Each simulation took approximately 30 s.

Results and Discussion

Fig. 1 shows fringes projected onto a sphere artefact. The fringes look curved in the camera perspective due to the form of the spheres. There is some specular reflection on the spheres and part of the spheres are occluded from the view of the projector. A sphere located in the back right corner is out of focus of the camera. The simulation of a similar scene is shown in Fig. 2, where a single sphere is simulated that increases its radius from 0.08 m to 0.12 m and 0.16 m. The curved fringes found in Fig. 1 are also present in Fig. 2. The specular reflection is not present because the surface is assumed to be Lambertian. Fig. 2 provides evidence that the model is capable of simulating the change in pattern due to surface topography.

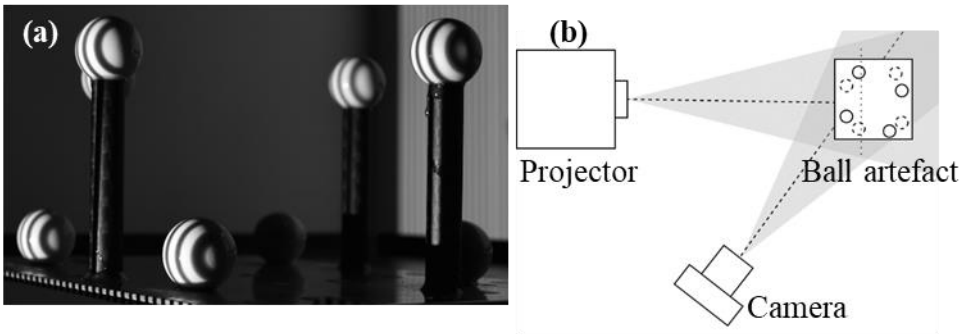

Fig. 1. (a) Image of a collection of 20 mm diameter optical spheres placed in the measurement volume of a fringe projection system. Configuration is shown graphically in (b).

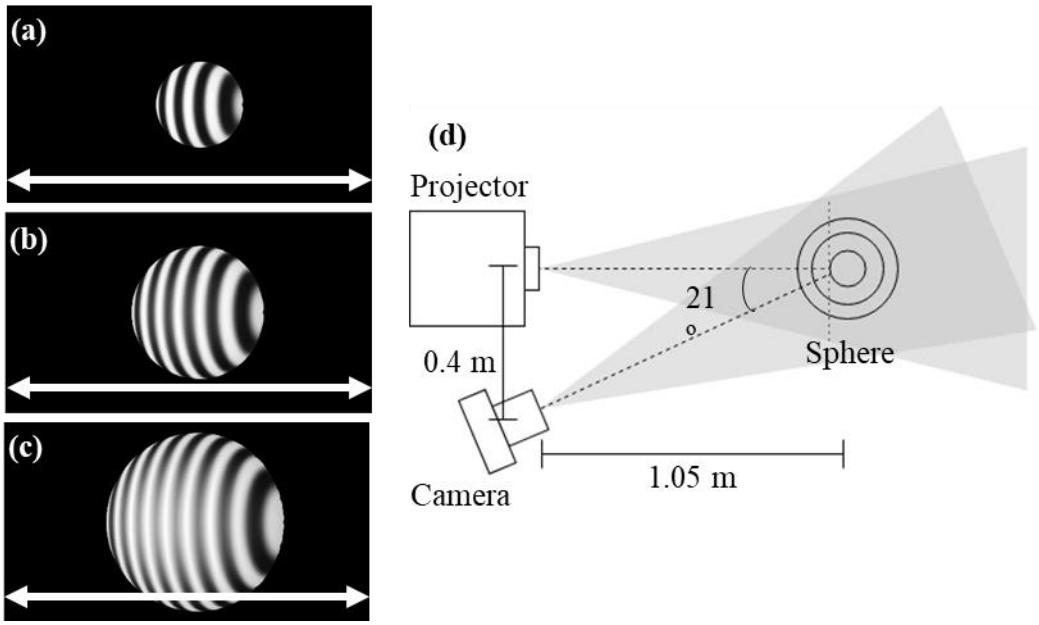

Fig. 2. Model scene of a sphere of increasing radius of 0.08 m, 0.12 m, 0.16 m for (a), (b) and (c) respectively. Configuration is shown graphically in (d). The dashed line represents the optical axis and the dotted line is the projector focal plane. Scale bar in (a-c) is 0.62 m.

Fig. 3 shows another image taken where the projector is placed at distances 1.23 m, 0.89 m and 0.66 m from the surface, with the surface and camera position fixed. In Fig. 3, the surface undergoes a magnification. Fig. 3(c) the surface is no longer located in the depth of focus and becomes blurred. Fig. 4 shows a simulation of a scene that includes a surface that is both in and out of focus. The surface closest to the projector (right) is brighter and compressed compared to the surface that is furthest away (left). Fig. 4 shows that the model presented here can qualitatively recreate the effect of focus and magnification found in a fringe projection system, which cannot be done using a two-dimensional linear model or a geometrical model only.

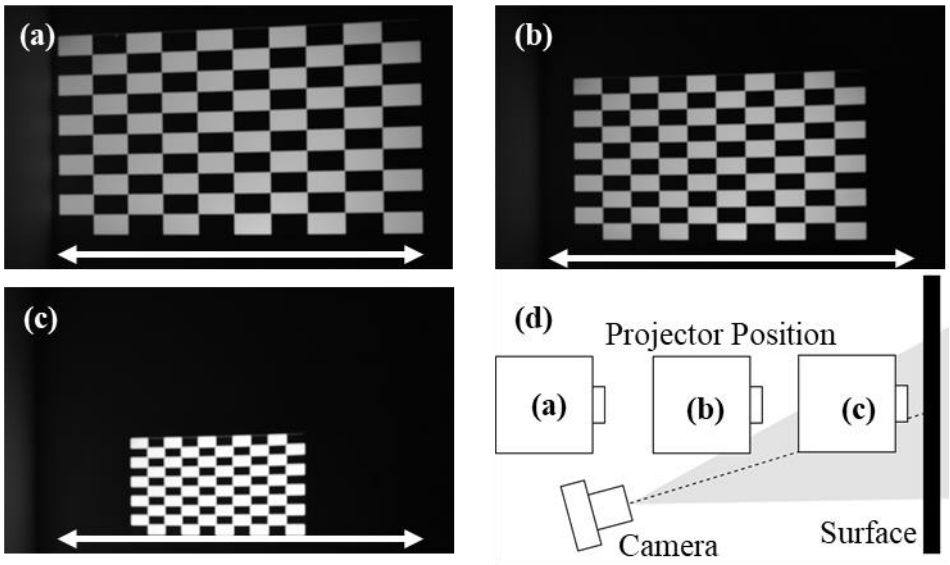

Fig. 3. (a-c) images of a proceeding projector with camera and surface static, with (c) being the furthest distance from projector to surface and (a) being the closest. Configuration is shown graphically in (d). The scale bar represents a length of 64 cm on the surface.

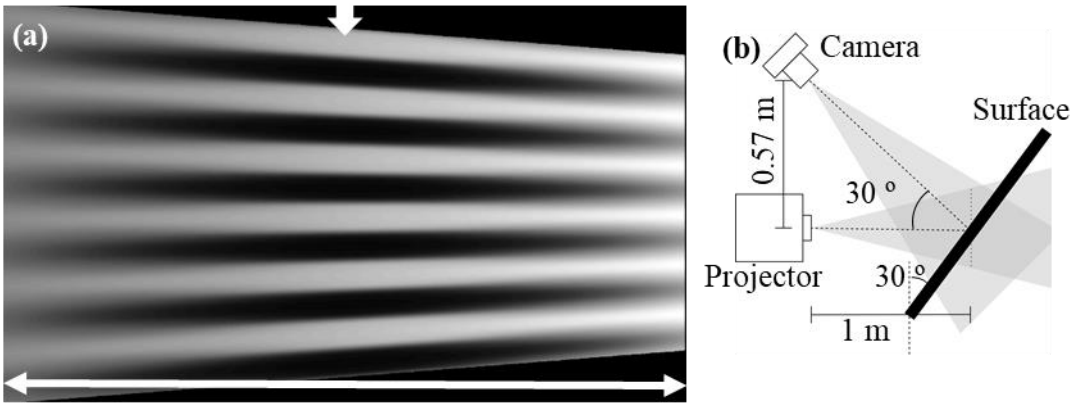

Fig. 4. Model scene of a surface placed at 45° to the optical axis of the projector. The downward arrow and scale bar in (a) represent the projectors focal plane location and a distance of 0.66 m respectively. Configuration is shown graphically in (b), with the dotted line representing the focal plane of the projector.

Conclusion

We have modelled fringe projection by combining 3D imaging theory with a geometric transformation. The preliminary results show that projection image distortion caused by surface topography and diffraction effects can be described by this model. Qualitative agreements with experiments were achieved. The potential advantage of this modelling approach is the inclusion of surface scattering/diffraction effects and using the OTF as a metric to evaluate and compare the performance of competing fringe projection systems. In future work, surface-light interactions will be included within the model. The model will continue to be developed for use in a Monte-Carlo framework that can evaluate uncertainty in fringe projection systems.

References

[1] A. Chatterjee, P. Singh, V. Bhatia, and S. Prakash, Ear biometrics recognition using laser biospeckled fringe projection profilometry. Opt. Laser. Technol., 2019. 112: p. 368-378.
[2] W. He, K. Zhong, Z. Li, X. Meng, X. Cheng, X. Liu, and Y. Shi, Accurate calibration method for blade 3D shape metrology system integrated by fringe projection profilometry and conoscopic holography. Opt. Laser. Eng., 2018. 110: p. 253-261.
[3] S. Zhang, High-speed 3D shape measurement with structured light methods: A review. Opt. Laser. Eng., 2018. 106: p. 119-131.
[4] S. Feng, Y. Zhang, Q. Chen, C. Zuo, R. Li, and G. Shen, General solution for high dynamic range three-dimensional shape measurement using the fringe projection technique. Opt. Laser. Eng., 2014. 59: p. 56-71.
[5] ISO 15530: Geometrical product specifications (GPS) - Coordinate measuring machines (CMM): Technique for determining the uncertainty of measurement, 2013
[6] ISO 25178: Geometrical product specifications (GPS) - Surface texture: Areal, 2019
[7] M. Gupta, A. Agrawal, A. Veeraraghavan, and S.G. Narasimhan, A practical approach to 3D scanning in the presence of interreflections, subsurface scattering and defocus. Int. J. Comput. Vis., 2013. 102(1-3): p. 33-55.
[8] L. Rao and F. Da, Local blur analysis and phase error correction method for fringe projection profilometry systems. Appl. Opt., 2018. 57(15): p. 4267-4276.
[9] C. Waddington and J. Kofman, Analysis of measurement sensitivity to illuminance and fringe-pattern gray levels for fringe-pattern projection adaptive to ambient lighting. Opt. Laser. Eng., 2010. 48(2): p. 251-256.

[10] N. Southon, P. Stavroulakis, R. Goodridge, and R.K. Leach, In-process measurement and monitoring of a polymer laser sintering powder bed with fringe projection. Mater. Des., 2018. 157: p. 227-234.
[11] A. Inanç, G. Kösoğlu, H. Yüksel, and M.N. Inci, 3-d optical profilometry at micron scale with multi-frequency fringe projection using modified fibre optic lloyd's mirror technique. Opt. Laser. Eng., 2018. 105: p. 14-26.
[12] H. Du, X. Chen, J. Xi, C. Yu, and B. Zhao, Development and Verification of a Novel Robot-Integrated Fringe Projection 3D Scanning System for Large-Scale Metrology. Sensors, 2017. 17(12): p. 2886.
[13] M. Ribo and M. Brandner. State of the art on vision-based structured light systems for 3D measurements. in ROSE. 2005. IEEE.
[14] N. Vukašinović, D. Bračun, J. Možina, and J. Duhovnik, The influence of incident angle, object colour and distance on CNC laser scanning. Int. J. Adv. Manuf. Tech., 2010. 50(1-4): p. 265-274.
[15] B. Zhang, A. Davies, C. Evans, and J. Ziegert, Validity of the instrument transfer function for fringe projection metrology. Appl. Opt., 2018. 57(11): p. 2795-2803.
[16] K. Haskamp, M. Kästner, C. Ohrt, and E. Reithmeier, Estimation of measurement uncertainties using virtual fringe projection technique. Appl. Opt., 2012. 51(10): p. 1516-1520.
[17] R. Su, M. Thomas, R.K. Leach, and J. Coupland, Effects of defocus on the transfer function of coherence scanning interferometry. Opt. Lett., 2018. 43(1): p. 82-85.
[18] J.M. Coupland and J. Lobera, Holography, tomography and 3D microscopy as linear filtering operations. Meas. Sci. Technol., 2008. 19(7): p. 074012.
[19] R. Su, Y. Wang, J. Coupland, and R.K. Leach, On tilt and curvature dependent errors and the calibration of coherence scanning interferometry. Opt. Express, 2017. 25(4): p. 3297-3310.
[20] N. Streibl, Three-dimensional imaging by a microscope. JOSA A, 1985. 2(2): p. 121-127.

Acknowledgements

We would like to thank the Engineering and Physical Sciences Research Council (Grants EP/L01534X/1 and EP/M008983/1) and Liam Bradley-Smith of the Manufacturing Technology Centre (Coventry, UK).